https://doi.org/10.58195/iaet.v3i1.150

Global Science Publishing

IAET

Innovations in Applied Engineering and Technology

https://ojs.sgsci.org/journals/iaet

Article

Experimental Study on the Performance of Frictional Drag Reducer with Low Gravity Solids

Yuxi Jia [1], Jihu Lei [2,*]

[1] *The University of Tulsa, Tulsa, OK 74104, USA*

[2] *Haldor Topsoe (Beijing) Co.,Ltd, Beijing 100025, China*

Abstract: Reducing energy consumption during drilling operations is beneficial to both the environment and economy. Frictional drag reducers (FDR) are widely used to reduce the energy loss caused by turbulent flow. FDR plays an important role in flow lines as they can reduce the frictional pressure drop effectively, and benefit the selection of circulating fluid and pump. However, several factors can influence the performance of FDR, including fluid additives and incorporated solids, such as drill solids. Thus, the main objective of this paper is to study the influence of low gravity solids (LGS) on the performance of the FDR. This paper is mainly based on experimental study. The experimental work contains two parts: rheology characterization and flow loop tests. Rheology characterization tests were performed to calculate the flow consistency index (K) and flow behavior index (n). Flow loop experiments were conducted for two geometry (0.457 inch and 0.797 inch diameter). Xanthan gum was used as a fractional drag reducer. Bentonite and quartz sand were added as low gravity solids. Three designed water-based mud systems are tested for drag reduction efficiency of Xanthan gum. Flow rate of the mud varied from 3 gpm to 16 gpm. Concentration of Xanthan ranged from 0.1 lbm/bbl to 0.6 lbm/bbl. Low weight solids were added with weight percentage of 0.5%, 1%, 2% and 2.5%. The result shows that xanthan gum is an efficient drag reducer for adequate reasons. Firstly, even at al low concentration, xanthan gum shows high resistance to degradation. Secondly, the maximum drag reduction with xanthan gum is up to 70.54% with a concentration of 0.6 lbm/bbl. However, the existence of different low gravity solids influence the efficiency of xanthan gum in different styles. Experiment results indicate that the higher the weight percentage of bentonite, the lower the drag reduction effectiveness. While with the increasing concentration of quartz sand, the drag reduction does not show an intense change. This study intents to give an instructive guidance on usage of frictional drag reducers in drilling mud system design. Removal of low gravity solids from the mud is difficult, which pose a danger to the drilling fluid. By understanding the effectiveness of FDR, we can reduce energy consumption when irremovable low gravity solids exist. FDR can be used for modifying the mud contents to develop a lower pressure gradient under turbulent flow condition. In the same scenario, adding FDR can suppress turbulent at a constant pressure gradient but with a higher flow rate.

Keywords: energy consumption reduction; xanthan gum; drag reducer; friction factor; pressure loss

1. Introduction

Reducing energy consumption during drilling operations is beneficial to both the environment and the

Received: 8 February 2024; Accepted: 7 March 2024.

* Corresponding: Email address: fjl@topsoe.com

economy. Therefore, frictional drag reducers have been utilized widely in the field. Reduction in drag will benefit the process of drilling, cementing, as well as enhance oil recovery [1–4]. However, several factors can influence the effectiveness of frictional drag reducers, including fluid additives and incorporated solids such as low gravity solids.

Despite the important, beneficial role of frictional drag reducers, very little work has been done to investigate the potential effect of low gravity solids on drag reducers. Determining the influence of low-gravity drill solids on the performance of drag reducers is anticipated to yield a number of important advantages related to conventional and horizontal drilling. Performing controlled experiments to study the extent to which various fluid additives and incorporated LGS affect the performance of the friction drag reduction will enable us to optimize the drilling process and save money in the long run.

The aim of the study is to investigate the drag reduction effectiveness of xanthan gum when different concentration of low gravity solid are added to the flow. The goal of these experiments is to measure the frictional pressure drop in the test sections at different concentrations of LGS, and all the experiments are carried out using fresh water to eliminate the effect of other substances. Xanthan gum has been selected as the polymer to be used as the frictional drag reducer. We have tested xanthan gum solution at different pipe sizes in the Dynamic Testing Facility and analyzed the data. The concentration of 0.4lbm/bbl, which appears to be the concentration at which maximum drag reduction achieved for xanthan gum solution has been selected for clay contamination tests. Two kinds of low gravity solids, i.e., bentonite (as a chemically active LGS) and quartz sand (as an inert LGS), were selected to be added to the 0.4 lbm/bbl xanthan gum solution. The flow loop experiments were conducted for different weight percentages of low gravity solids at the same temperature. For each weight percentage, the solutions were pumped through two different diameter pipes in order to study the pipe diameter influence on drag reduction. The effect of weight percentage of the low gravity solid additives, the effect of flow rate, and the effect of pipe diameter on the performance of frictional drag reduction were analyzed.

Generally, the Prandtl-Karman coordinate ($1/\sqrt{f}$ versus $Re\sqrt{f}$) which is shown in Figure 1 is used to present the drag reduction data since Prandtl-Karman law for Newtonian turbulent pipe flow is a straight line in these coordinates in a semi-logarithmic diagram. For Newtonian turbulent pipe flow, the usual Blasius law is shown in equation (1), where f is the friction factor and Re is the Reynolds number.

$$\frac{1}{\sqrt{f}} = 4.0\, log_{10}\left(Re\sqrt{f}\right) - 4.0 \tag{1}$$

The approximate relation for the regime with drag reduction is shown in equation (2), where δ is the slope increment, the difference between polymer solution and solvent slopes on the Prandtl-Karman coordinates.

$$\frac{1}{\sqrt{f}} = (4.0+\delta)\, log_{10}\left(Re\sqrt{f}\right) - \delta log_{10}(Re\sqrt{f})_0 \tag{2}$$

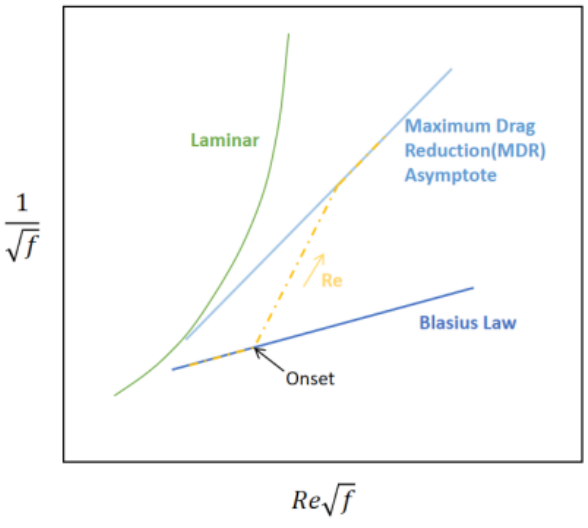

Figure 1. Prandtl-Karman coordinates.

If the friction drag for pipe flows is plotted in Prandtl-Karman coordinates (Figure 1), the point at which the solution line departure from the Prandtl-Karman law (or Blasius law) can determined as the onset of drag reduction [5–8].

The theoretical interpretation of the onset of the drag reduction is called time criterion [9,10]. The criterion may be split into several parts. First, drag reduction occurs when the polymer relaxation time is longer than the time scale of the near-wall turbulence, i.e. $T_z > \frac{\mu_s}{\rho u_\tau^2}$, where $T_z$is the average time it takes for a stretched polymer to return to a coiled configuration [11]. The ratio of the polymer time scale to the flow time scale of the near-wall turbulence, defined as the wall-shear Weissenberg number. Under most circumstances, the onset of drag reduction is when the Weissenberg number equals one. Second, whenever this condition is satisfied, the polymer molecules become substantially stretched. This is called the coil-stretch transition. In this extended state, the elongational viscosity increases by a factor of the order of ten thousand (e.g. Metzner & Metzner [12]). Third, this phenomenal increase in elongational viscosity manifests preferentially near the wall because the extensional strain rates are the highest there. Finally, it is supposed that the increased elongational viscosity suppresses turbulent fluctuations, increases the buffer layer thickness and reduces wall friction. Lumley [9], for instance, produced detailed arguments to show that these considerations are plausible (see, also, Virk et al. [10]). The explanations of detailed onset of drag reduction can be divided into two groups, elastic effect [11 – 17], and viscous effect [18, 19]. These two theories are fundamentally different. However, both have merits when compared to the experimental data.

The onset of the drag reduction can be affected by multiple factors such as polymer concentration, molecular weight, random coil size and solvent viscosity. Wall shear stress and polymer random-coil size are respectively the flow and polymeric parameters most relevant to on-set. The presence of high polymer concentration can induce the early occurrence of turbulent flow. Hansen et al. [18] and Forame et al. [19] experimentally found that the early turbulent flow can occur with dilute polymer fluids in large diameter pipes. Samanta et al. [20] experimentally showed that with a moderate concentration of polymer, the chaotic flow will start at the Reynolds number below that which is needed for turbulent flow. Instead of relating the early occurrence of turbulent flow solely to the Toms phenomena as Hansen et al. [10] and Forame et al. [21] did, Samanta et al. [22] suggested that the elastic instability induced by the polymer is the essential reason why the early turbulent flow occurs.

In the petroleum industry, drag reduction agents are widely used, and have been added to the fluid during the processes of oil well fracturing operations, enhanced oil recovery, pipeline transportation of crude oil and refining petroleum products [23 – 36]. The use of drag reducing additives helps drilling fluids develop a lower pressure gradient at a constant flow rate under turbulent flow conditions. At a constant pressure gradient, a treated mud will flow faster than an untreated mud because turbulence is suppressed. Adding a drag reducer to a drilling fluid can reduce the high pump pressure loss due to hydraulic friction. The inclusion of drag reducer in completion and workover brines can smooth the operation and reduce energy consumption. Drag reducers can reduce the energy consumption in long distance transportation, which is one of the most energy consuming sectors faced by the oil and gas industry. The turbulence inside the transported fluid makes the fluid particles move in a chaotic manner which redirects the pumping energy to multiple directions, and causes high skin fraction. Drag is the pressure head losses inside a pipe that cause the flow rate to decrease. To overcome the decreasing flow rate, more pumping stations are installed along the pipeline to supply energy and uphold the desired flow rate. The addition of drag reducers will reduce the number of the pumps or pumping stations needed during transportation. Pipelines are also used to transport solid products in the petroleum industry [37 –51].

2. Experimental Work

2.1. Flow loop

Flow loop experiments were conducted on a flow loop system called the Dynamic Testing Facility (DTF). The DTF is an indoor facility that contained several flow loops, Figures 2 and 3 show the schematic of the DTF

facility. The section we used was a relatively small-scale flow loop, the flow was driven by a 125-psi Moyno progressive cavity pump. The Moyno progressive cavity pump have the advantage of minimizing the influence of the pump on the polymer. Volumetric flow rate was measured by a Micro Motion flow meter and temperature was monitored by sensors located in various location.

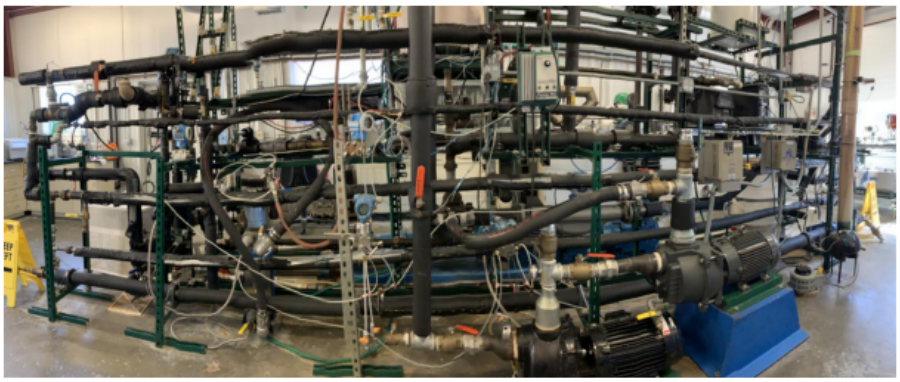

Figure 2. Schematic of the Dynamic Testing Facility.

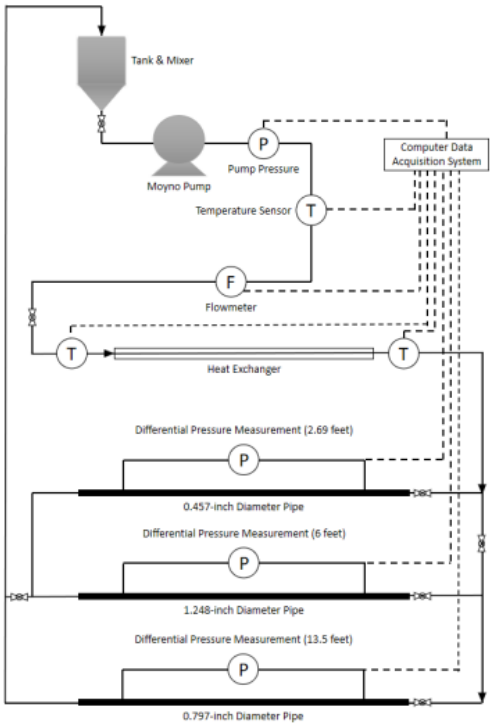

Figure 3. Schematic representation of the Dynamic Testing Facility.

2.2. Test Matrix

Experiments can be divided into three groups:

(1) The first group used the solution of fresh water and xanthan gum;

(2) The second group used the solution of fresh water, xanthan gum and bentonite;

(3) The third group used the solution of fresh water, xanthan gum and quartz sand.

The flow loop experiments were firstly conducted with different concentrations of xanthan gum and fresh water solutions. After that, based on the results obtained from the xanthan gum experiments, two kinds of low gravity solids were added to the xanthan gum solution. The concentration of the xanthan gum solution stayed constant, and low gravity solids were added with respectively different weight percentages. The two kinds of low gravity solids were decided to be bentonite and quartz sand (170-350 micron), the former one is chemically active, and the second one is inert. Test matrices for these three groups of experiments are given in the following

Table 1 to Table 3.

Table 1. Test matrix for xanthan gum experiments.

Pipe Diameter (inch)			**0.457**			
Concent. (lbm/bbl)	0.1	0.2	0.3	0.4	0.5	0.6
Flow Rate (gpm)	3–16gpm	3–16gpm	3–16gpm	3–16gpm	3–16gpm	3–16gpm
Pipe Diameter (inch)				0.797		
Concent. (lbm/bbl)	0.1	0.2	0.3	0.4	0.5	0.6
Flow Rate (gpm)	3–19gpm	3–19gpm	3–19gpm	3–19gpm	3–19gpm	3–19gpm
Temp ('F)				71±0.5		

As Tables 2 and 3 show, when adding different concentrations of LGS, the concentrations of xanthan gum were all 0.4lbm/bbl. It was because after conducting experiments with polymer solution. We found that, in the appropriate flow rate range, the optimum concentration of xanthan gum is 0.4 lbm/bbl. In order to ensure the consistency of the results, the temperature of the fluid has been maintained at 71 (plus or minus 0.5) degrees Fahrenheit during the experiments.

Table 2. Test matrix for quartz sand and xanthan gum experiments.

Pipe Diameter (inch)		**0.457**		
%Quartz Sand Weight Percentage	0.5	1	2	2.5
Flow Rate (gpm)	3–16gpm	3–16gpm	3–16gpm	3–16gpm
Pipe Diameter (inch)		0.797		
%Quartz Sand Weight Percentage	0.5	1	2	2.5
Flow Rate (gpm)	3–19gpm	3–19gpm	3–19gpm	3–19gpm
Temp ('F)		71±0.5		
Xanthan Gum Concentration (lbm/bbl)		0.4		

Table 3. Test matrix for bentonite and xanthan gum experiments.

Pipe Diameter (inch)			**0.457**			
%Bentonite Weight Percentage	0.5	1	1.5	2	2.5	3
Flow Rate (gpm)	3–16gpm	3–16gpm	3–16gpm	3–16gpm	3–16gpm	3–16gpm
Pipe Diameter (inch)			0.797			
%Bentonite Weight Percentage	0.5	1	1.5	2	2.5	3

Cont.

Flow Rate (gpm)	3–19gpm	3–19gpm	3–19gpm	3–19gpm	3–19gpm	3–19gpm
Temp ('F)	71±0.5					
Xanthan Gum Concentration (lbm/bbl)	0.4					

3. Results and Discussion

3.1. Xanthan Gum Experiments

3.1.1. Xanthan gum experiment results

In xanthan gum experiments, 6 different concentration of xanthan gum solutions have been tested in two different size pipes, Figure 4 shows the pressure drop gradient over the test section versus flow rate in the 0.457-inch diameter pipe, and Figure 5 shows the pressure drop gradient over the test section versus flow rate in the 0.797-inch diameter pipe.

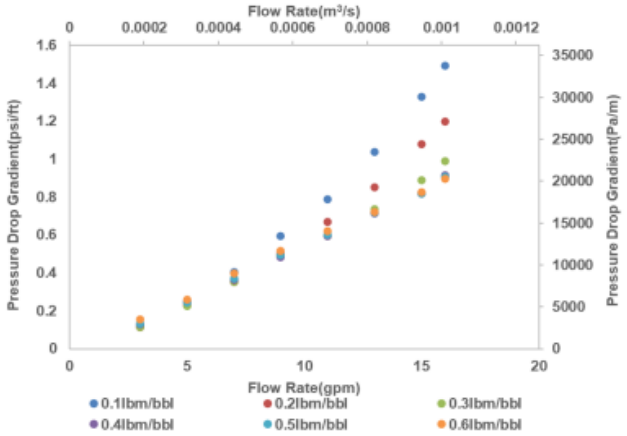

Figure 4. Tested pressure drop gradient versus flow rate in 0.457-inch diameter pipe with xanthan gum.

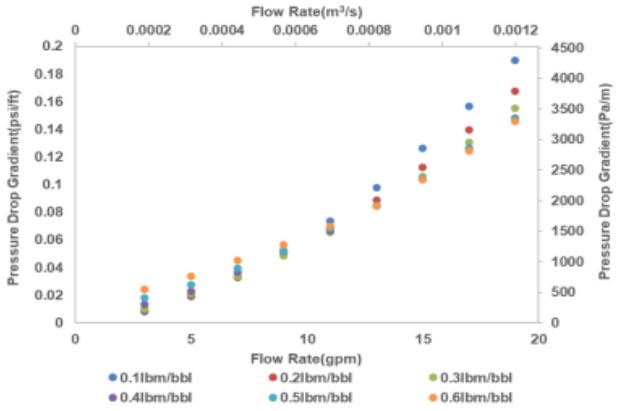

Figure 5. Tested pressure drop gradient versus flow rate in 0.797-inch diameter pipe with xanthan gum.

As Figures 4 and 5 indicate, in 0.457-inch diameter pipe and 0.7970inch diameter pipe, the pressure drop gradients were observed to have similar behaviors. As the concentration of xanthan gum increasing, the influence of flow rate on pressure drop gradient reduces, for example, in 0.457-inch diameter pipe, the difference between the pressure drop gradients at 3 gpm and 16 gpm with 0.1lbm/bbl xanthan gum solution is

1.38 psi/ft, but the difference for 0.6lbm/bbl xanthan gum solution is 0.74 psi/ft. Also, the gaps between the pressure drop gradient for different concentrations at a certain flow rate are gradually decreasing. Which means, the pressure drop gradients stop to change with different concentration after a certain concentration.

3.1.2. Xanthan gum experiment discussions

The drag reduction values were calculated and plotted in Figures 6 and 7. Figure 6 shows the drag reduction versus flow rate in 0.457-inch diameter pipe. As the figure directly shows, at the flow rate of 3 gpm, the drag reduction effect with 0.6lbm/bbl.

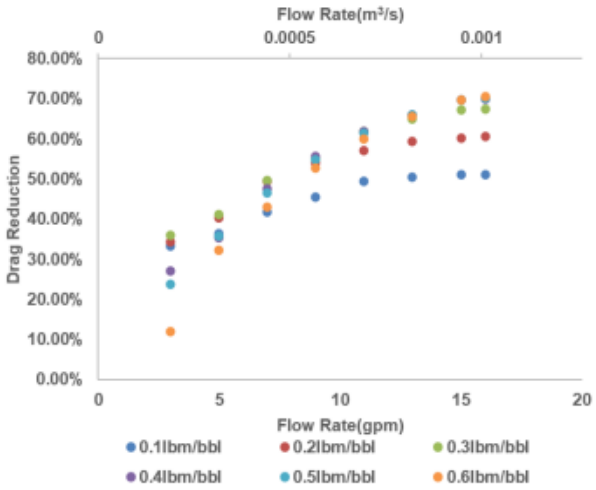

Figure 6. Drag reduction versus flow rate in 0.457-inch diameter pipe with xanthan gum.

Xanthan gum concentration is the lowest among all. However, at the flow rate of 16 gpm, the drag reduction effect is the highest. For the 0.1lbm/bbl xanthan gum solution, the situation is the opposite. This implies that for higher concentration polymer solutions, the drag reduction effect is more sensitive to the flow rate. The concentration of xanthan gum will also affect the gap between drag reduction for a certain flow rate. For example, at the flow rate of 15 gpm, the gap between drag reduction with xanthan gum concentration of 0.1lbm/bbl and 0.2lbm/bbl is 9.2%, and the gap between 0.3lbm/bbl and 0.4lbm/bbl is 2.49%, i.e., with the increasing concentration, the gap becomes smaller. In 0.457-inch diameter pipe, the maximum drag reduction occurs at the flow rate of 16 gpm, the maximum drag reduction is 70.54%.

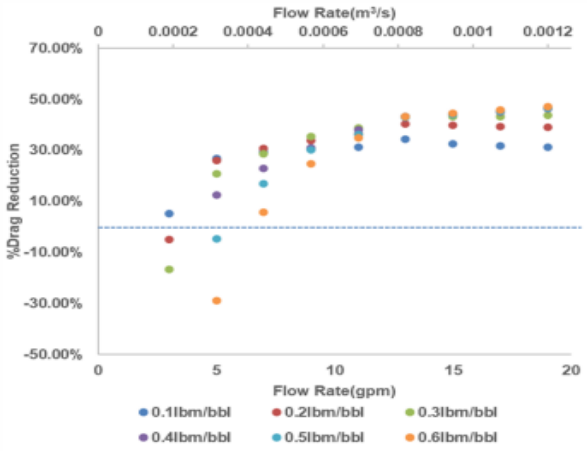

Figure 7. Drag reduction versus flow rate in 0.797-inch diameter pipe with xanthan gum.

Figure 7 shows the drag reduction versus flow rate in 0.797-inch diameter pipe, the drag reduction show the

similar behaviors as observed in the smaller size pipe. The effect of the concentration of xanthan gum on the onset of the drag reduction is that, with the increase of concentration, the onset of drag reduction is delayed, and this kind of effect can be explained by the viscosity difference. When the concentration of xanthan gum is high, the viscosity of the solution also becomes higher, which causes the turbulence not sufficient (or even no turbulent) at low flow rate. It also explains that for low flow rates, such as 3 gpm, a low concentration of xanthan gum has a better drag reduction effect than the high concentrations.

We tested different concentrations of xanthan gum solutions in flow loop, and proved that the xanthan gum solution had a drag reduction effect under turbulent flow. At the same time, we also found an optimum xanthan gum concentration for the next step of the experiments. To show the drag reduction effect of different concentration of xanthan gum solution better and more clearly, the drag reduction effects versus xanthan gum concentration at certain flow rates in 0.457-inch diameter pipe and in 0.797-inch diameter pipe are plotted in respectively Figures 8 and 9.

Figure 8 indicates that, in 0.457-inch diameter pipe, the higher the flow rate, the higher overall drag reduction effect. Also, before a certain concentration, the higher the concentration of xanthan gum, the better the drag reduction effect, but the drag reduction stop increasing after that certain concentration which is 0.4lbm/bbl. The curves in the Figure 9 are similar to the previous one, After the concentration of 0.4lbm/bbl, the increase of drag reduction effect abruptly stop. In the sum of all the above analyses, 0.4lbm/bbl will be the optimum concentration of xanthan gum in this flow loop.

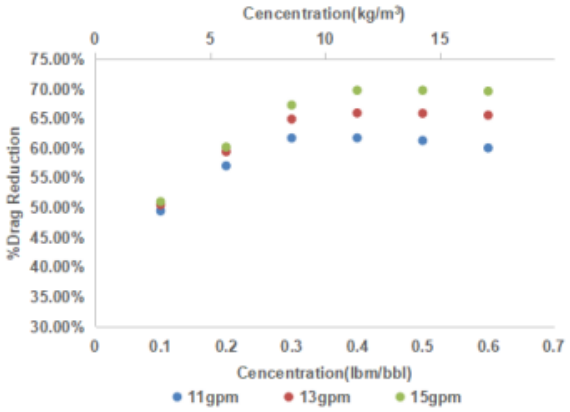

Figure 8. Drag reduction versus concentration in 0.457-inch diameter pipe at the same flow rate with xanthan gum solution.

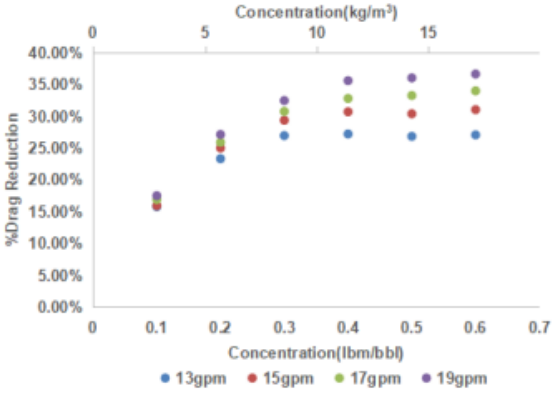

Figure 9. Drag reduction versus concentration in 0.797-inch diameter pipe at the same flow rate with xanthan gum solution.

In Figures 10 and 11, the Reynolds number-friction factor correlations were plotted, and the friction factors were calculated from experimental frictional pressure losses. The relationship between friction factor and Reynolds number in both diameter pipes show similar behavior. With the increasing concentration, the coefficients of the trend line are increasing, and the index is decreasing (based on Equation A.1). This indicates that, for low concentration of xanthan gum solution, the friction factor are less sensitive to flow rate changing, while with higher concentration, the sensitivity increases. Also, at the same Reynolds number, friction factors tend to decrease with the increasing concentration of the xanthan gum.

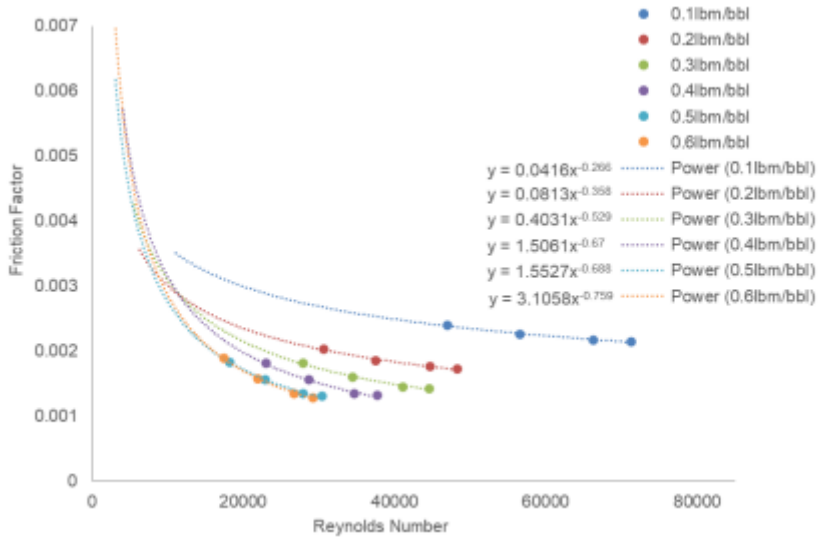

Figure 10. Friction Factor-Reynolds number correlation in 0.457-inch diameter pipe with xanthan gum solution.

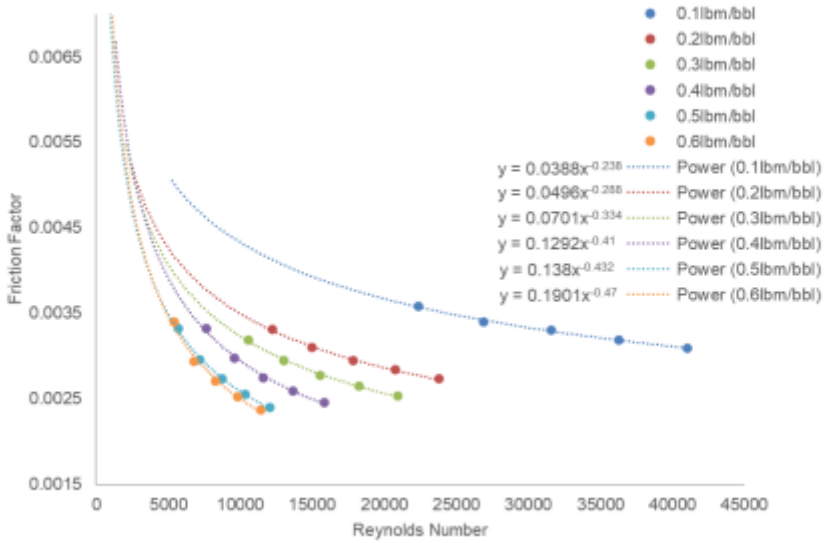

Figure 11. Friction Factor-Reynolds number correlation in 0.797-inch diameter pipe with xanthan gum solution.

After comparing the results for the xanthan gum flow loop experiments, conclusions can be drawn.

(1) With the increase of the xanthan gum concentration, viscosity of the solution will also increase.

(2) Drag reduction effect will increase with the increase of concentration of xanthan gum.

(3) Compared to other concentrations, when the concentration is 0.4lbm/bbl, xanthan gum shows the best Drag reduction. As a result, it can be said that the optimum concentration of xanthan gum to be used in the current flow loop is 0.4lbm/bbl.

3.2. Quartz Sand and Xanthan Gum Experiments

3.2.1. Quartz sand and xanthan gum experiment results

Quartz sand has been added to the xanthan gum solution with weight percentage of 0.5%, 1%, 2% and 2.5%. The pressure drop gradient versus flow rate for both pipe sizes are plotted in Figures 12 and 13.

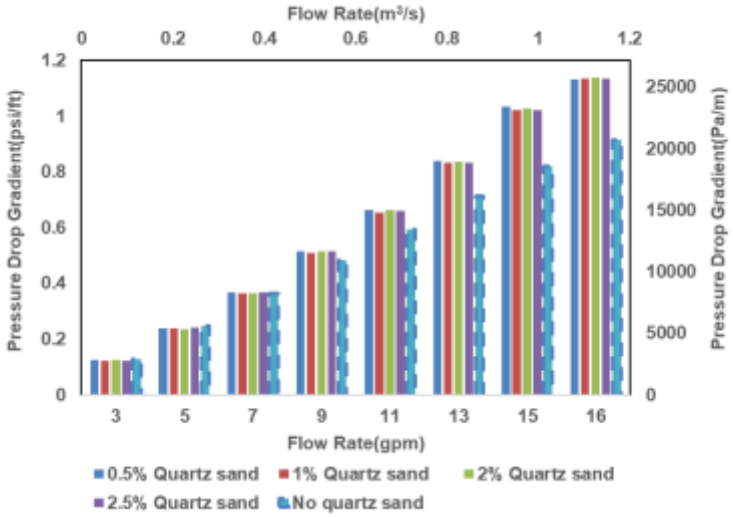

Figure 12. Tested pressure drop gradient versus flow rate in 0.457-inch diameter pipe with quartz sand and xanthan gum solution.

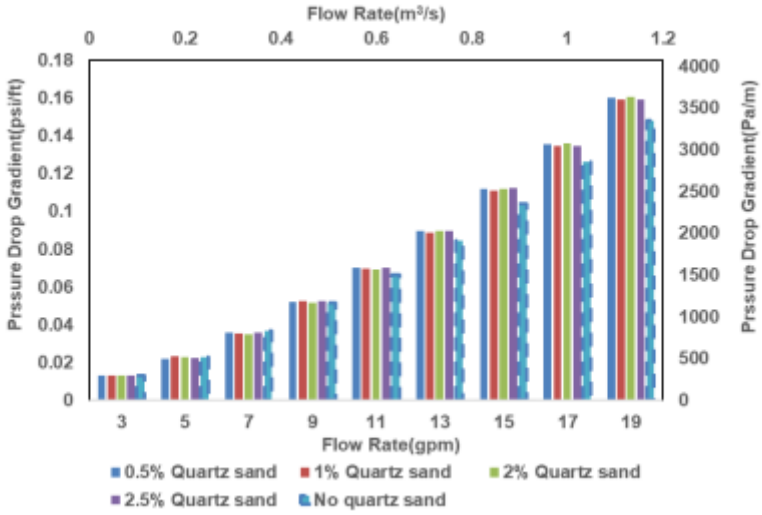

Figure 13. Tested pressure drop gradient versus flow rate in 0.797-inch diameter pipe with quartz sand and xanthan gum solution.

For a constant flow rate, the pressure drop gradients at different weight percentages of quartz sand remained almost the same (differences are within 3%) for both pipe sizes. The light blue bars with dashed lines in the figures represent the pressure drop gradient when there is no quartz sand existing in the xanthan solution. The pressure drop gradient of xanthan gum solution is slightly smaller than the pressure drop gradient of quartz sand and xanthan gum solutions. However, at low flow rates, the difference is hard to detect. The xanthan gum solution that we used was a 0.4 lbm/bbl solution, so the viscosity alone might not be sufficient to suspend all the quartz sand particles. However, when the flow rate is high enough, the quartz sand might be picked up due to excessive turbulence, and the pressure drop gradients were thus affected. Please note that for all the data points

(except 3 gpm in 0.797-inch diameter pipe) are theoretically in the turbulent flow regime.

3.2.2. Quartz sand and xanthan gum experiment discussion

The drag reduction has been calculated and plotted in the Figures 14 and 15.

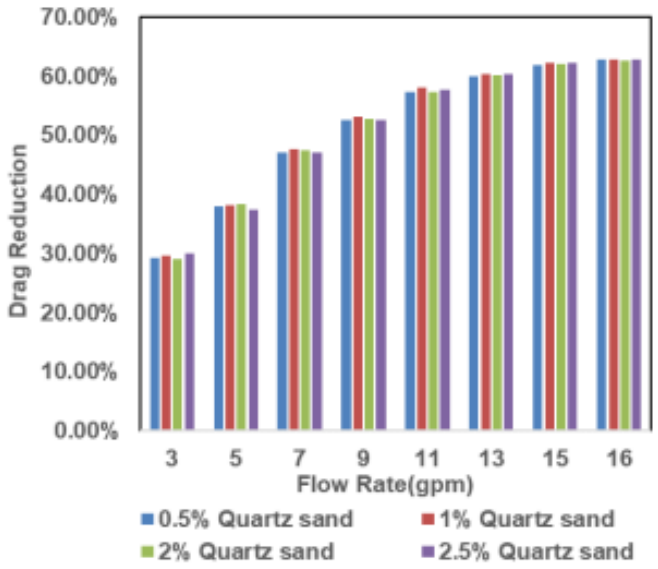

Figure 14. Drag reduction versus flow rate in 0.457-inch diameter pipe with quartz sand and xanthan gum solution.

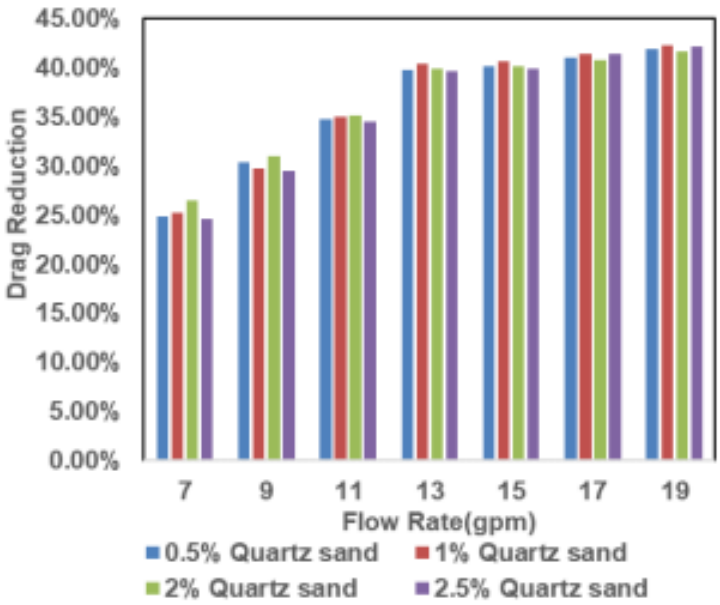

Figure 15. Drag reduction versus flow rate in 0.797-inch diameter pipe with quartz sand and xanthan gum solution.

As the figures show, for certain flow rates and pipe sizes, the drag reduction of different quartz sand weight percentages did not change. The relationship between the Reynolds number and friction factor was plotted in Figures 16 and 17 for 0.457-inch and 0.797-inch diameter pipes, respectively. It appears that the friction factors for different weight percentages of quartz sand are similar.

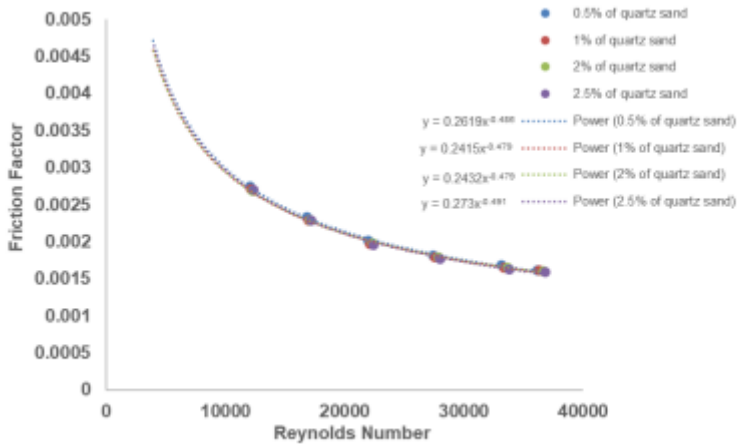

Figure16. Friction factor versus Reynolds number with quartz sand and xanthan gum solution in 0.457-inch diameter pipe.

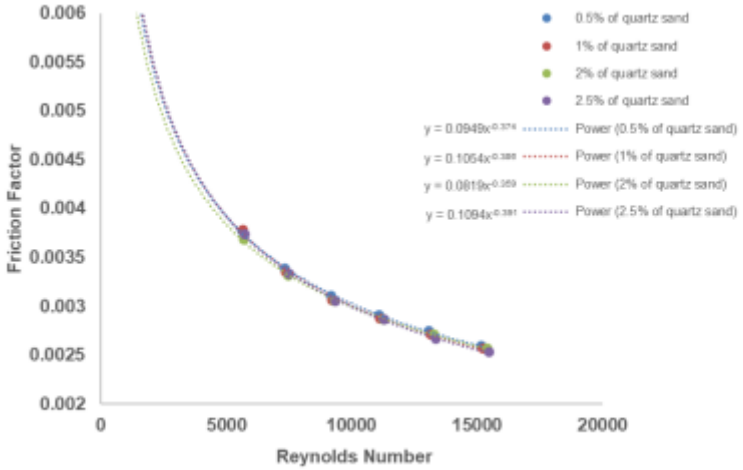

Figure17. Friction factor versus Reynolds number with quartz sand and xanthan gum solution in 0.797-inch diameter pipe.

The results from the xanthan gum and quartz sand experiments revealed that the inactive (or inert) solids have insignificant or no effect on frictional drag reduction. Here are the conclusions.

(1) The drag reduction effect of xanthan gum is not sensitive to the concentration of quartz sand. In a suitable quartz sand weight percentage range, the pressure reduction is, in fact, almost constant.

(2) Flow rate has a positive effect on drag reduction effect. Increased flow rate increased the pressure reduction effect due to higher turbulence. Drag reduction eventually reaches a plateau, i.e., further increase in flow rate does not cause any increase in drag reduction.

3.3. Bentonite and Xanthan Gum Experiments

3.3.1. Bentonite experiment results

To calculate the drag reduction for each concentration of bentonite and xanthan gum solution used during the experiments, the baseline experiments of bentonite solution were conducted. As the test matrix shows, six different concentrations of bentonite and xanthan gum solutions were tested. Therefore, the baseline tests were conducted with six different concentrations of bentonite solutions. For each experiment, 15 gallons of fluid was prepared, and the old fluid was discarded and prepared from scratch. The observed pressure drop gradient versus flow rate and average fluid velocity are presented in Figures 18 and 19.

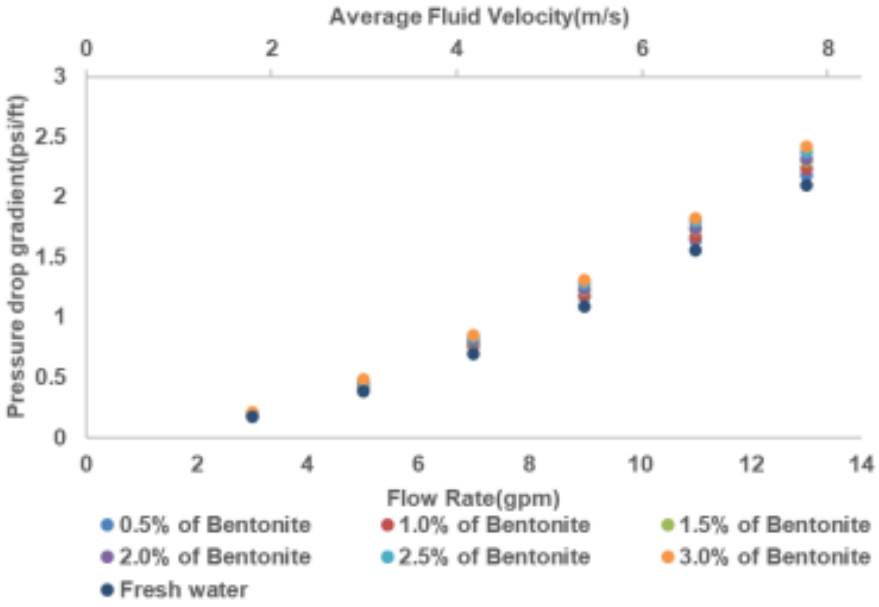

Figure 18. Tested pressure drop gradient versus flow rate and average fluid velocity in 0.457-inch diameter pipe with bentonite solution.

With the increase of the weight percentage of the bentonite, the apparent viscosity of the solution is increasing, along with the pressure drop gradient.

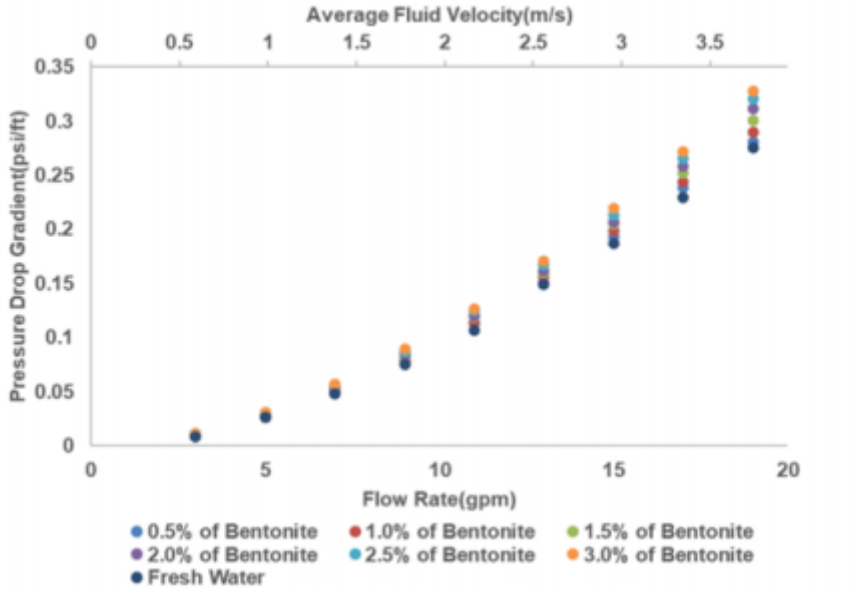

Figure 19. Tested pressure drop gradient versus flow rate and average fluid velocity in 0.797-inch diameter pipe with bentonite solution.

3.3.2. Bentonite and xanthan gum experiment results

Figure 20 shows the tested pressure drop gradient versus flow rate in 0.457-inch diameter pipe with different weight percentages of bentonite. It can be observed that with the increasing weight percentage of bentonite, the pressure drop gradient becomes larger. The dark blue triangles stand for the pressure drop gradient when only xanthan gum exits in the flow. The pressure drop gradient in the polymer solution without bentonite added is the lowest among all the other solutions with bentonite added. Also, the figure shows that the difference in pressure drop gradient at different concentrations is smaller at lower flow rates.

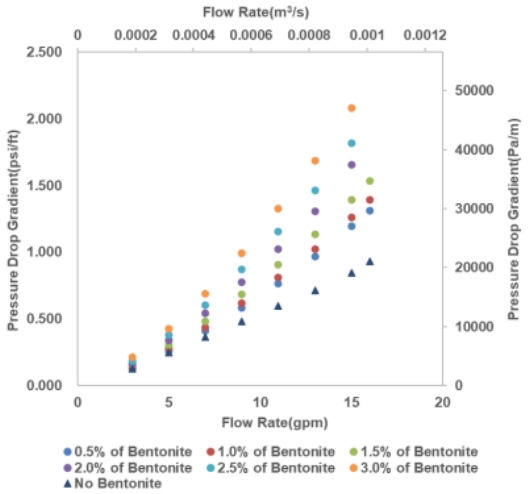

Figure 20. Tested pressure drop gradient versus flow rate in 0.457-inch diameter pipe with bentonite and xanthan gum solution.

Figure 21 shows the pressure drop gradient with different weight percentages in 0.797-inch diameter pipe, the pressure drop gradient in 0.797 inch ID pipe shows a similar behavior as observed in the smaller size pipe. Less difference is observed between pressure drop gradient of different weight percentages of bentonite at low flow rates. A relatively higher difference between the pressure drop gradients of different weight percentages of bentonite is observed at high flow rates. The overall pressure drop gradients with no bentonite added are less than those with bentonite.

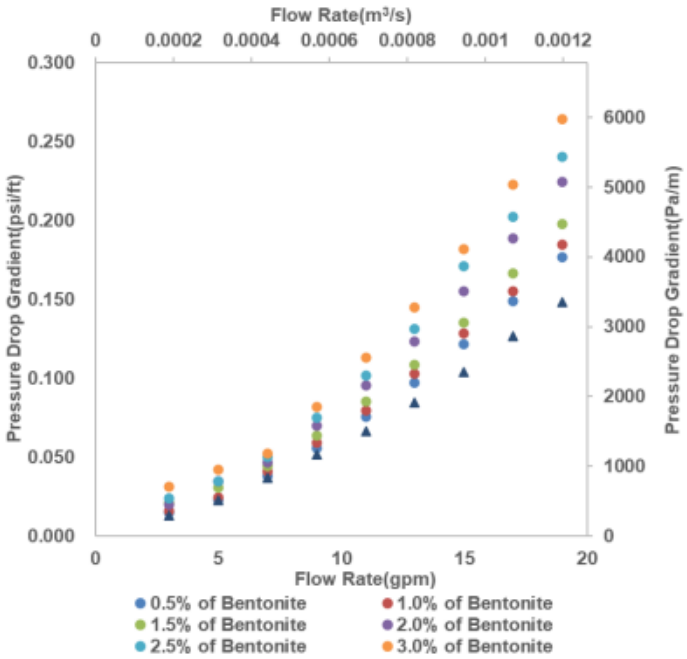

Figure 21. Tested pressure drop gradient versus flow rate in 0.797-inch diameter pipe with bentonite and xanthan gum solution.

3.3.3. Bentonite and xanthan gum experiment discussions

Based on the rheological properties of the bentonite and xanthan gum solution, the theoretical pressure drop gradients were calculated. To better illustrate the relationship among the pressure drop gradient for xanthan gum solution with or without bentonite, they were plotted on Figures 22 and 23.

In Figures 22 and 23, each plot shows the theoretical and tested pressure drop gradients versus flow rate

with and without bentonite at a certain weight percentage of bentonite. As the figures show, theoretical pressure drop gradients with bentonite added are higher than the theoretical pressure drop gradients without bentonite. This is because the apparent viscosity of the xanthan gum solution with bentonite is higher than the one without bentonite. The tested pressure drop gradient of xanthan gum with bentonite is always the smallest.

From Figures 22 and 23, it is worth noticing that with the increasing weight percentage of bentonite, the distance between the data points of tested and theoretical pressure drop gradients for the same flow rate are decreasing. This means that as the concentration of bentonite gets higher, the difference between the tested and theoretical pressure drop gradients get smaller.

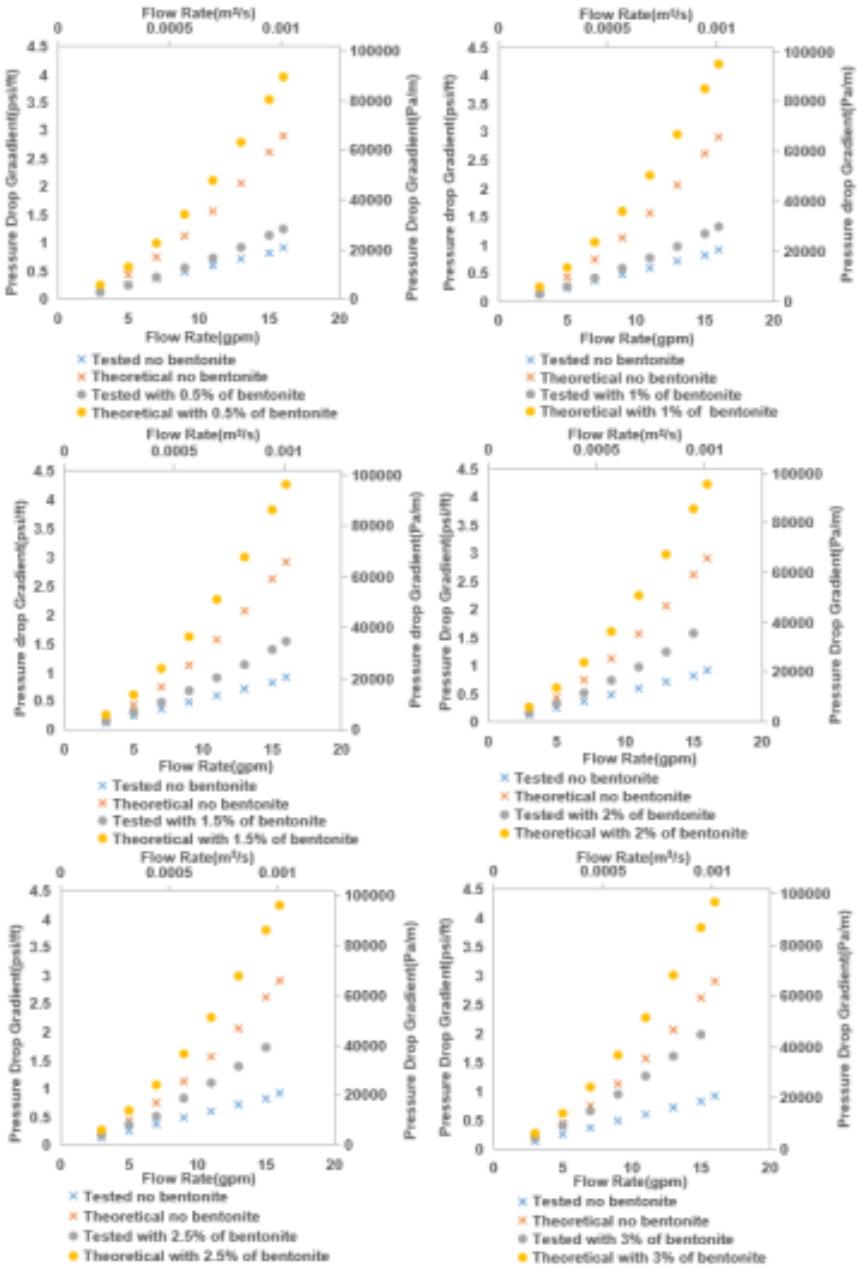

Figure 22. Tested and theoretical pressure drop gradient in 0.457-inch diameter pipe with or with without bentonite.

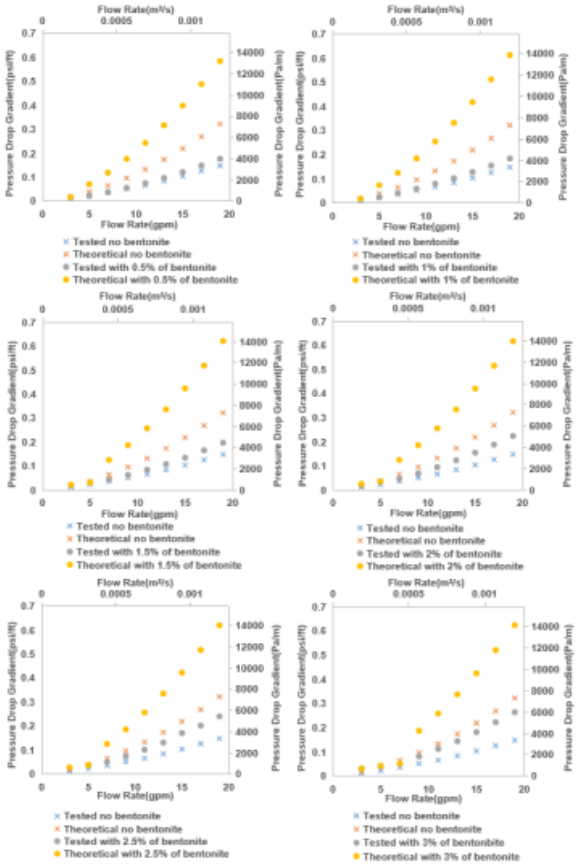

Figure 23. Tested and theoretical pressure drop gradient in 0.797-inch diameter pipe with or with without bentonite.

Figure 24 shows the drag reduction effect versus flow rate and average fluid velocity in the 0.457 inch diameter pipe. As the flow rate becomes higher, the increase of drag reduction effect starts to slow down. However, with the increasing bentonite concentration, the increase slows down even faster. The DR of 0.4 lbm/bbl xanthan gum solution was higher than all the xanthan gum solutions with bentonite. With the increase of concentration of bentonite in xanthan gum solution, the drag reduction effect is restricted. From 0.5% of bentonite to 1.5% of bentonite, the effect of bentonite on xanthan gum is not significant. In other words, the drag reduction effect is similar and/or noticeable for bentonite concentrations up to 1.5%. However, when the concentration exceeds 1.5%, the drag reduction effect starts to be negatively affected by the presence of excessive bentonite. The drag reduction continuously decreases as the bentonite concentration increases.

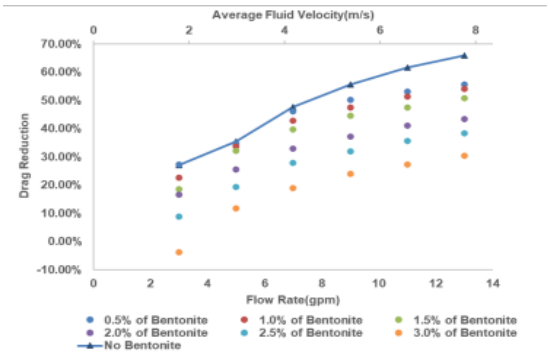

Figure 24. Drag Reduction versus flow rate and average fluid velocity in 0.457-inch diameter pipe with bentonite and xanthan gum solution.

In Figure 25, the drag reduction versus bentonite weight percentage was plotted. In this figure, it can be seen that the drag reduction effect significantly drops as the bentonite concentration increases.

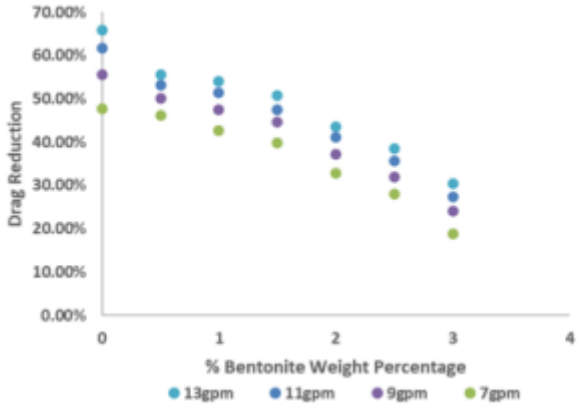

Figure 25. Drag Reduction versus bentonite weight percentage in 0.457-inch diameter pipe with bentonite and xanthan gum solution.

We also analyzed the data acquired from the 0.797-inch diameter pipe in a similar way. In Figure 26, the drag reduction versus flow rate and average fluid velocity in 0.797-inch diameter pipe is plotted. A similar behavior as observed in the 0.457-inch diameter pipe can be determined. The growth rate of drag reduction with the xanthan gum solution is greater than that of drag reduction with the bentonite and xanthan gum solution. This indicates that the presence of bentonite does affect the performance of xanthan gum. Similarly, bentonite concentrations up to 1.5% show similar drag reduction performance. With the increase in the weight percentage of bentonite, the drag reduction effect is restricted further.

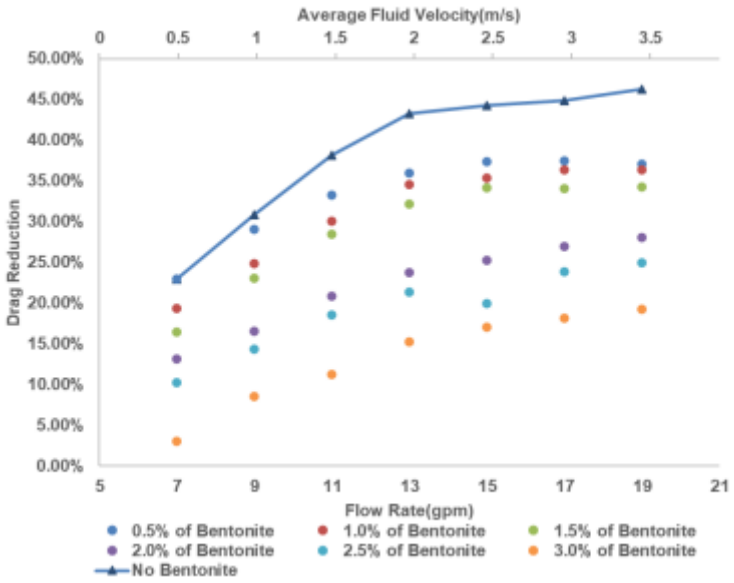

Figure 26. Drag Reduction versus flow rate and average fluid velocity in 0.797-inch diameter pipe with bentonite and xanthan gum solution.

In Figure 27, the drag reduction versus bentonite weight percentage was plotted. In this figure, a similar behavior is observed as in the 0.457-inch diameter pipe, i.e. as the flow rates are increased, the drag reduction reduces significantly. When bentonite concentration is greater than 1.5%, drag reduction decreased substantially. The relationship between the Reynolds number and friction factor were plotted in Figures 28 and 29. In both figures, it appears that the friction factors seem to be similar for bentonite weight percentages up to 1.5%.

However, as the weight percentage increases, the friction factor increases as well (for the same Reynolds number), which indicates that higher bentonite concentrations will cause higher frictional pressure losses. Also, for the same Reynolds number the friction factor of blue" x" markers, representing xanthan gum solution, are lower than the others.

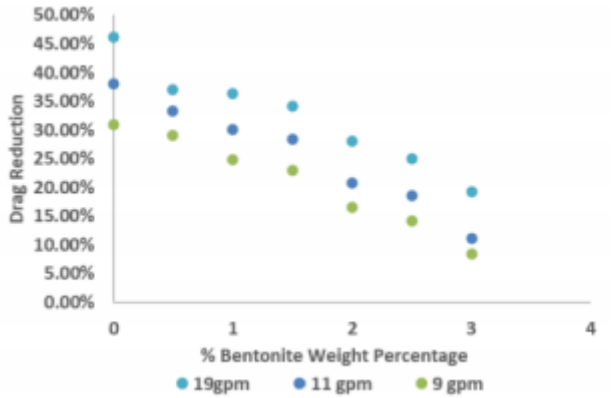

Figure 27. Drag reduction versus bentonite weight percentage in 0.797-inch diameter pipe with bentonite and xanthan gum solution.

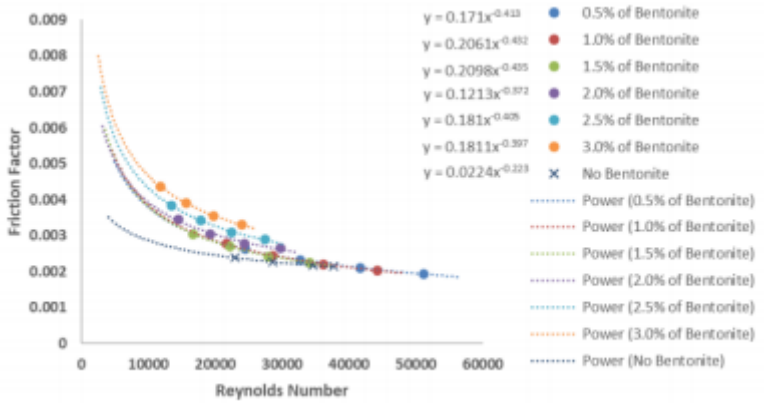

Figure 28. Reynolds number versus Fanning friction factor for bentonite and xanthan gum solution in 0.457-inch diameter pipe.

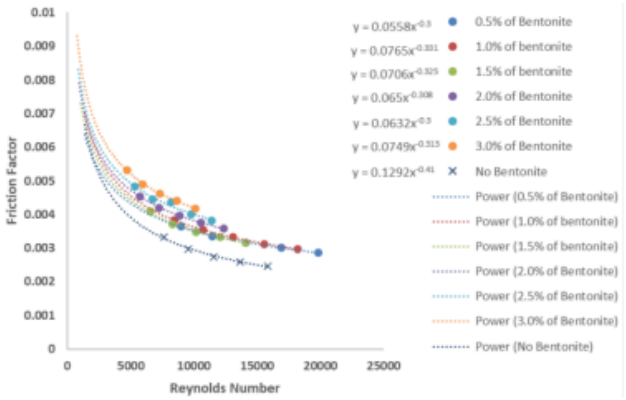

Figure 29. Reynolds number versus Fanning friction factor for bentonite and xanthan gum solution in 0.797-inch diameter pipe.

4. Conclusions

Xanthan gum shows a very good drag reduction effect. The maximum drag reduction achieved with xanthan gum was 70.54% with a concentration of 0.6lbm/bbl. When the concentration is above 0.4lbm/bbl, the drag reduction at relatively high flow rate almost remains unchanged.

Overall, the drag reduction in xanthan gum solution with low gravity solids added are lower than that in xanthan gum solution. This suggested that the presence of low gravity solid will affect the turbulence structure in fluids and cause suppression in drag reduction, or that, they may adsorb the polymer additives.

With the increasing concentration of quartz sand, the drag reduction does not show a big change. However, with the increasing weight percentage of bentonite, the drag reduction reduces more and more intensely. This discrepancy suggests that the presence of low gravity solids in the system will affect the effectiveness of polymer. However, the effect of chemically active and adsorptive low gravity solid, bentonite, to the effectiveness of polymer is more related to the LGS weight percentage.

With the increasing weight percentage of bentonite, the drag reduction effect is more restricted. At first, the restriction was not big, which means the drag reduction was still similar. However, when the weight percentage exceeds 1.5%, the decrease of drag reduction abruptly increases. This observed behavior is consistent with previous field experience, in which the drag reduction will be most affected when the weight percentage of the low gravity solid is above 2%.

The maximum drag reduction achieved with xanthan gum and bentonite solution was 55.59% with a bentonite weight percentage of 0.5%. The maximum drag reduction achieved with xanthan gum when quartz sand exists was 62.82% with a bentonite weight percentage of 0.5%. With the same weight percentage, bentonite can further reduce the effectiveness of xanthan gum. Moreover, data analysis methods represented in can be further leveraged to improve this work.

Funding

Not applicable.

Author Contributions

Conceptualization, Y.J. and J.L.; writing—original draft preparation, Y.J. and J.L.; writing—review and editing, Y.J. and J.L.; All of the authors read and agreed to the published the final manuscript.

Institutional Review Board Statement

Not applicable.

Informed Consent Statement

Not applicable.

Data Availability Statement

Not applicable.

Conflicts of Interest

The authors declare no conflict of interest.

References

1 Zheng D, Ozbayoglu E, Miska SZ, Liu Y, Li Y. Cement Sheath Fatigue Failure Prediction By ANN-Based Model. In Offshore Technology Conference, Houston, TX, USA, 2–5 May 2022.

2 Zheng D, Ozbayoglu EM, Miska SZ, Liu Y. Cement Sheath Fatigue Failure Prediction By Support Vector Machine Based Model. SPE Eastern Regional Meeting, Wheeling, WV, USA, 18–20 October 2022.

3 Liu Y, Upchurch ER, Ozbayoglu EM, Baldino S, Zheng D, Wang J. Gas Migration Model for Non-

Newtonian Fluids under Shut-in Well Conditions. *SPE/IA*DC Drilling Conference and Exhibition, Stavanger, Norway, 7–9 March 2023.

4 Liu Y, Upchurch ER, Ozbayoglu EM, Baldino S, Wang J, Zheng D. Design and Calculation of Process Parameters in Bullheading and Pressurized Mud Cap Drilling. SPE/IADC Drilling Conference and Exhibition, Stavanger, Norway, 7–9 March 2023.

5 Luo C, Cao Y, Liu Y, Zhong S, Zhao S, Liu Z, Liu Y, Zheng D. Experimental and Modeling Investigation on Gas-Liquid Two-Phase Flow in Horizontal Gas Wells. *Journal of Energy Resources Technology* 2023; **145** (**1**): 013102.

6 Ke W, Zeng H, Wang Z, Yu H, Liu Y, Zheng D, Zhu J, Zhu H. A Numerical Study on Labyrinth Screw Pump (LSP) Performance under Viscous Fluid Flow. *Energies* 2023; **16**(**16**): 5997.

7 Zhu H, Liu Y, Tychus D, Zheng D, Adiraju S, Tatu J, Zhu J, Zhang H. Sensitivity Analysis on Tailpipe Design for Mitigating Terrain Slug in Horizontal Wells. *Geoenergy Science and Engineering* 2024; **235**(**2**): 212598.

8 Virk PS. Drag Reduction Fundamentals. *AIChE Journal* 1975; **21**(**4**): 625–656.

9 Lumley JL. Drag Reduction in Turbulent Flow By Polymer Additives. *Journal of Polymer Science: Macromolecular Reviews* 1973; **7**(**1**): 263–290.

10 Hershey HC, Zakin JL. A Molecular Approach to Predicting the Onset of Drag Reduction in the Turbulent Flflow of Dilute Polymer Solutions. *Chemical Engineering Science* 1967; **22**: 1847–1857.

11 Zimm BH. Dynamics of Polymer Molecules in Dilute Solutions: Viscoelasticity, Flow Birefringence and Dielectric Loss. *The Journal of Chemical Physics* 1956; **24**: 269–79.

12 Metzner AB, Metzner AP. Stress Levels in Rapid Extensional Flows of Polymeric Fluids. *Rheologica Acta* 1970; **9**(**2**): 174–181.

13 Virk PS, Merrill EW, Mickley HS, Smith KA, Mollo-Christensen EL. The Toms Phenomenon: Turbulent Pipe Flow of Dilute Polymer Solutions. *Journal of Fluid Mechanics* 1967; **30**(**2**): 305–328.

14 De Gennes PG. *Introduction to Polymer Dynamics*; Cambridge University Press: Cambridge, UK, 1990.

15 Tabor M, De Gennes PG. A Cascade Theory of Drag Reduction. *EPL (Europhysics Letters)* 1986; **2**(**7**): 519.

16 Sreenivasan KR, White CM. The Onset of Drag Reduction By Dilute Polymer Additives, and the Maximum Drag Reduction Asymptote. *Journal of Fluid Mechanics* 2000; **409**: 149–164.

17 Zheng D, Miska SZ, Ozbayoglu E. The Influence of Formation Creeping on Wellbore Integrity. SPE 2021 Symposium Compilation, Virtual, 26 November 2021.

18 Zheng D, Miska Z, Ozbayoglu, Zhang Y. The Influence of Elliptical-Geometry Wellbore on Zonal Isolation. 56th U.S. Rock Mechanics/Geomechanics Symposium, Santa Fe, NM, USA, 26–29June 2022.

19 L'vov VS, Pomyalov A, Procaccia I, Tiberkevich V. Drag Reduction By Polymers in Wall Bounded Turbulence. *Physical review letters* 2004; **92**(**24**): 244503.

20 Lumley JL. Drag Reduction By Additives. *Annual Review of Fluid Mechanics* 1969; **1**: 367–84.

21 Ryskin G. Turbulent Drag Reduction By Polymers: a Quantitative Theory. *Physical review letters* 1987; **59** (**18**): 2059.

22 Hansen RJ, Little RC. Early Turbulence and Drag Reduction Phenomena in Larger Pipes. *Nature* 1974; **252**: 690.

23 Forame PC, Hansen RJ, Little RC. Observations of Early Turbulence in the Pipe Flow of Drag Reducing Polymer Solutions. *AIChE Journal* 1972; **18**: 213–217.

24 Samanta D, Dubief Y, Holzner M, Sch¨afer C, Morozov A N, Wagner C, Hof B. Elasto-Inertial Turbulence. *Proceedings of the National Academy of Sciences* 2013; **110**(**26**): 10557–10562.

25 Zheng D, Miska S, Ziaja M, Zhang J. Study of Anisotropic Strength Properties of Shale. *AGH Drilling Oil Gas* 2019; **36**(**1**): 93–112.

26 Zheng D, Ozbayoglu E, Miska S, Zhang J. Experimental Study of Anisotropic Strength Properties of Shale. In ARMA US Rock Mechanics/Geomechanics Symposium, Atlanta, GA, USA, 25–28 June 2023.

27 Rafieepour S, Zheng D, Miska S, Ozbayoglu E, Takach N, Yu M, Zhang J. Combined Experimental and Well Log Evaluation of Anisotropic Mechanical Properties of Shales: An Application to Wellbore Stability

in Bakken Formation. *SPE Annual Technical Conference and Exhibition,* Virtual, 26–29 October 2020.

28 Wang J, Ozbayoglu E, Baldino S, Liu Y, Zheng D. Time Series Data Analysis with Recurrent Neural Network for Early Kick Detection. Offshore Technology Conference, Houston, TX, USA, 1–4 May 2023.

29 Zheng D, Miska S, Ozbayoglu E, Zhang J. Combined Experimental and Well Log Study of Anisotropic Strength of Shale. SPE Annual Technical Conference and Exhibition, San Antonio, TX, USA, 16 – 18 October 2023.

30 Peng C, Pang J, Fu J, Cao Q, Zhang J, Li Q, Deng Z, Yang Y, Yu Z, Zheng D. Predicting Rate of Penetration in Ultra-Deep Wells Based on Deep Learning Method. *Arabian Journal for Science and Engineering* 2023; **48**(**12**): 16753–16768.

31 Zheng D, Ozbayoglu E, Miska S, Silvio B, Liu Y, Wang J. The Influence of Casing Eccentricity on Zonal Isolation. In ARMA US Rock Mechanics/Geomechanics Symposium, Atlanta, GA, USA, 25–28 June 2023.

32 Lin R, Yu Z, Zhao J, Ren L, Wu J, Wu J, Song Y, Zheng D. Cluster Spacing Optimization of Deep Shale Gas Fracturing With Non-Uniform Geostress. *Petroleum Science and Technology* 2022; 1 – 18. DOI: 10.1080/10916466.2022.2148694.

33 Chen X, Shi Z, Zheng D. Application of Pre-Stack Elastic Impedance Inversion to Metamorphic Reservoir Prediction in JZ25-1 Oilfield. *Editorial Department of Petroleum Geology and Recovery Efficiency* 2015; **22** (**4**): 69–73.

34 Ren L, Yu Z, Zheng D, Lin R, Xie M. Towards Intelligent Shale-Gas Horizontal Well Fracturing: Neural Network and Particle Swarm Optimization for Predicting the Test Production of Shale Gas Horizontal Well. Energy in Data Conference, Austin, TX, USA, 20–23 February 2022.

35 Guo S, Li Y, Chen T, Zheng D, Du J, Bu Y, Zhou A, Pang X, Liu H. Controlling the Hydration Rate of Alkali-Activated Slag By the Slow Release of NaOH. *Geoenergy Science and Engineering* 2023; **228**: 211960.

36 Zheng, Danzhu, Turhan, Cinar, Wang, Ningyu, Ashok, Pradeepkumar, and Eric van Oort. Prioritizing Wells for Repurposing or Permanent Abandonment Based on Generalized Well Integrity Risk Analysis. IADC/SPE International Drilling Conference and Exhibition, Galveston, TX, USA, 5–7March 2024.

37 Liu Y, Upchurch ER, Ozbayoglu EM, Baldino S, Zheng D, Wang J. Prediction of Rise Velocity of Taylor Bubbles in Pipes Using an Artificial Neural Network. *Authorea.* January 16, 2024. DOI: 10.22541/au.170536908.87694225/v1.

38 Yang Bi, Shenglai Guo, Tian Chen, Danzhu Zheng, Kai Wang, Yuhuan Bu, Huajie Liu. Preparation and Characteristics of a pH Intelligent Response Blocking Agent for the Microcrack in the Cement Sheath. *ACS Omega* 2023; **8**(**39**):36284–36291. DOI: 10.1021/acsomega.3c04865.

39 Luo Z, Xu H, Chen F. Audio Sentiment Analysis by Heterogeneous Signal Features Learned from Utterance-Based Parallel Neural Network. Proceedings of the 2nd Workshop on Affective Content Analysis (AffCon 2019) co-located with Thirty-Third AAAI Conference on Artificial Intelligence (AAAI 2019), Honolulu, HI, USA, 27 January 2019.

40 Chen F, Luo Z, Xu Y, Ke D. Complementary Fusion of Multi-Features and Multi-Modalities in Sentiment Analysis. AAAI-2020 Workshop on Affective Content Analysis, New York, NY, USA, 7 February 2020.

41 Luo Z, Zeng X, Bao Z, Xu M. Deep Learning-Based Strategy for Macromolecules Classification with Imbalanced Data from Cellular Electron Cryotomography. 2019 International Joint Conference on Neural Networks (IJCNN), Budapest, Hungary, 14–19 July 2019.

42 Luo Z. Knowledge-guided Aspect-based Summarization. 2023 International Conference on Communications, Computing and Artificial Intelligence (CCCAI), Shanghai, China, 23–25 June 2023.

43 Tao G, Wang H, Shen Y, Zhai L, Liu B, Wang B, Chen W, Xing S, Chen Y, Gu HM, Qin S, Zhang DW. Surf4 Deficiency Reduces Intestinal Lipid Absorption and Secretion and Decreases Metabolism in Mice. *Arterioscler Thromb Vasc Biol* 2023; **43**(**4**): 562–580.

44 Shen Y, Gu HM, Qin S, Zhang DW. Surf4, Cargo Trafficking, Lipid Metabolism, and Therapeutic Implications. *J Mol Cell Biol*. 2022; **14**(**9**): mjac063.

45 Wang M, Alabi A, Gu HM, Gill G, Zhang Z, Jarad S, Xia X, Shen Y, Wang G, Zhang DW. Identification of

the Amino Acid Residues in the MT-Loop of MT1-MMP Critical for Its Ability to Cleave Low-Density Lipoprotein Receptor. *Frontiers in Cardiovascular Medicine* 2022; **9**: 917238.

46 Shen Y, Gu H, Zhai L, Wang B, Qin S, Zhang DW. The Role of Hepatic Surf4 in Lipoprotein Metabolism and the Development of Atherosclerosis in apoE -/- mice. *Biochim Biophys Acta Mol Cell Biol Lipids* 2022; **1867**(**10**): 159196.

47 Wang B, Shen Y, Zhai L, Xia X, Gu H-M, Wang M, Zhao Y, Chang X, Alabi A, Xing S, Deng S, Liu B, Wang G, Qin S, Zhang D-W. Atherosclerosis-Associated Hepatic Secretion of VLDL but Not PCSK9 Is Dependent on Cargo Receptor Protein Surf4. *J Lipid Res* 2021; **62**: 100091.

48 Deng SJ, Shen Y, Gu HM, Guo S, Wu SR, Zhang DW. The Role of the C-Terminal Domain of PCSK9 and SEC24 Isoforms in PCSK9 Secretion. *Biochim Biophys Acta Mol Cell Biol Lipids* 2020; **1865**(**6**): 158660.

49 Shen Y, Wang B, Deng S, Zhai L, Gu HM, Alabi A, Xia X, Zhao Y, Chang X, Qin S, Zhang DW. Surf4 Regulates Expression of Proprotein Convertase Subtilisin/Kexin Type 9 (PCSK9) but Is Not Required for PCSK9 Secretion in Cultured Human Hepatocytes. *Biochim Biophys Acta Mol Cell Biol Lipids* 2019; **1865** (**2**): 158555.

50 Dai W, Marieh F, Hamed GT, Hossein M, Loke KF. Application of Six Neural Network-Based Solutions on Bearing Capacity of Shallow Footing on Double-Layer Soils. *Steel and Composite Structures* 2023; **49**(**2**): 231–244.

51 Zhao Y, Dai W, Wang Z, Ragab AE. Application of Computer Simulation to Model Transient Vibration Responses of GPLs Reinforced Doubly Curved Concrete Panel Under Instantaneous Heating. *Materials Today Communications* 2023; **39**: 107949.